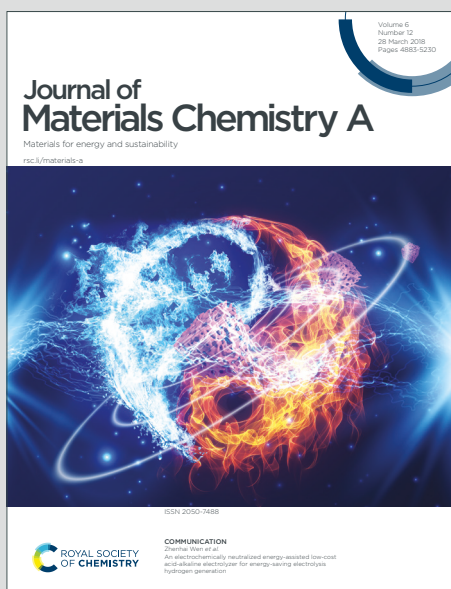


Journal of Materials Chemistry A

Materials for energy and sustainability

Accepted Manuscript

This article can be cited before page numbers have been issued, to do this please use: J. Shang, N. Kosem, Y. Kayo, X. Shen, S. Matsuyama, M. Watanabe, M. Inada, T. Ishihara and A. Staykov, *J. Mater. Chem. A*, 2025, DOI: 10.1039/D5TA05712D.



This is an Accepted Manuscript, which has been through the Royal Society of Chemistry peer review process and has been accepted for publication.

Accepted Manuscripts are published online shortly after acceptance, before technical editing, formatting and proof reading. Using this free service, authors can make their results available to the community, in citable form, before we publish the edited article. We will replace this Accepted Manuscript with the edited and formatted Advance Article as soon as it is available.

You can find more information about Accepted Manuscripts in the [Information for Authors](#).

Please note that technical editing may introduce minor changes to the text and/or graphics, which may alter content. The journal's standard [Terms & Conditions](#) and the [Ethical guidelines](#) still apply. In no event shall the Royal Society of Chemistry be held responsible for any errors or omissions in this Accepted Manuscript or any consequences arising from the use of any information it contains.

Improved Charge Transfer Performance of Eosin Y-Sensitized Anatase TiO₂ by Anchoring Group Modification: from the Theoretical Design to Experiment

Juan Shang,^{1,2,3,} Nuttavut Kosem,^{1,2} Yasuhiro Kayo,⁴ Xiao-Feng Shen,¹ Sayo*

Matsuyama,¹ Motonori Watanabe,^{1,2,4} Miki Inada,¹ Tatsumi Ishihara,^{1,2,4}

and Aleksandar Staykov^{1,2,}*

- 1) International Institute for Carbon-Neutral Energy Research (WPI-I2CNER), Kyushu University, Motooka 744, Fukuoka, 819-0395 Japan.
- 2) Mitsui Chemicals, Inc.-Carbon Neutral Research Center (MCI-CNRC), Kyushu University, Motooka 744, Fukuoka, 819-0395 Japan.
- 3) The Center for Energy Systems Design (CESD), International Institute for Carbon-neutral Energy Research (WPI-I2CNER), Kyushu University, 819-0395 Japan.
- 4) Department of Automotive Science, Kyushu University, Motooka 744, Fukuoka, 819-0395 Japan.

***Corresponding author**

*Juan Shang, E-mail: shang.juan.061@m.kyushu-u.ac.jp. Phone: +81-92-802-6717.

**Staykov Aleksandar, E-mail: alex@i2cner.kyushu-u.ac.jp. Phone: +81-92-802-6732.



ABSTRACT

Theoretical design and experimental proof of photocatalytic performance of Eosin Y (EY) on anatase TiO_2 with pyridine linker were performed for increasing photobiocatalytic activity of water splitting using visible light. Comparative studies on the hybrid interface of anatase and EY with the carboxyl and pyridine anchor were performed by density functional theory (DFT), time-dependent density functional theory (TD-DFT) calculations and experimental photoreduction of methyl viologen (MV). The geometries, binding interactions between dyes and anatase, electronic structures and electron transfer as well as the effect of isomers (ortho, meta, para) on the dye / anatase systems were investigated. Theoretical results indicated that EY with carboxyl and pyridine anchors had visible adsorption and electron transfer from the dye to the anatase titania. Compared to carboxyl-para, which had the best optical performance among carboxyl groups, the adsorption strength of pyridine-ortho was close to that of carboxyl-para, while the oscillator strength increased significantly, which was more than 10 times higher than that of carboxyl-para. Corresponding with the theoretical estimation, EY pyridine linked TiO_2 is active to MV reduction under visible light irradiation by fast charge transfer, in particular, pyridine-ortho and para. Furthermore, high stability is also achieved on pyridine-para. Apparent quantum yield higher than 2.00% and 0.67 % at 520 nm light was experimentally achieved on biocatalytic H_2 and NH_3 formation, respectively, on EY pyridine linked TiO_2 , which was correctly predicted by the DFT calculations.

1. INTRODUCTION

Energy transition, which involves reducing fossil fuel utilization and promoting the development of clean energies, is a crucial issue to mitigate the negative effect of climate change and to pursuit



a carbon-neutral society. Hydrogen is considered to be an ideal energy carrier due to its advantages of high specific energy density, purity, versatility, and possibilities for renewable production, etc.^{1,2} As a renewable secondary energy, hydrogen can be generated by many low-carbon-emission pathways such as electrolysis, electro-photolysis, radiolysis, thermo-chemical etc.^{3,4} In particular, solar-driven hydrogen production has gained significant attention because it provides a promising opportunity for renewable hydrogen energy so-called green hydrogen.

Since the photoelectrolysis method was proposed by Fujishima and Honda in 1972,⁵ researchers have steadily increased the attempts to directly harvest solar energy for efficient water electrolysis.^{6,7} In the photoelectrochemical water splitting systems the photocatalysts which use sunlight energy to dissociate water molecules into hydrogen and oxygen play a key role in the efficiency of hydrogen production.^{8,9} Anatase has been one of the most studied photocatalysts because of its appropriate position of conduction band (CB) edge (lower than the reduction energy of water, 0 V) and valence band (VB) edge (higher than the oxidation energy of oxygen, 1.23 V) to trigger the photoelectrochemical reaction.⁸⁻¹⁰ However, the band gap of anatase is ca. 3.20 eV which corresponds to ultraviolet (UV) light (only 3~4% of the solar energy).¹¹ Hence, it is important to narrow the band gap of anatase and to enhance its visible light response and photocatalytic activity.

To date, many modifications have been developed to improve the optical absorption of anatase including dopant introduction and dye sensitization. The dopants could be divided into metal and non-metal elements where metals were extensively investigated to act as a co-catalyst to increase the solar absorption. Some metals such as Au, Pt, Pd, Rh, Ni, etc., have been found to improve the photo electron-hole separation by trapping electrons at the interfaces of metal and anatase.^{10,12,13} For example, Murdoch et al.¹² found that Au-doped anatase showed a broader visible light absorption range and a high hydrogen production rate. This was due to the CB of Au was lower



than that of anatase, thereby the excited electrons accumulated at anatase could easily transfer to Au. The hydrogen ions trapped by Au at the interface with anatase enhanced the hydrogen molecule reduction activity. On the other hand, Au, Ni, Cu, Al, Ag, etc., were reported to promote visible light absorption due to the surface plasmon resonance (SPR) effect and localized surface plasmon resonance (LSPR) effect.^{9,14–17} These effects could increase the energy intensity of photo-excited electrons under visible light irradiation. Many studies of anatase doping with metal ions, Fe, Mo, Ru, Os, etc., and non-metal anions, N, F, P, S, Si, etc., attempt to modify the inherent bandgap of anatase TiO₂.^{10,18–22} Metal ion-doping could form impurity energy levels within the anatase bandgap, while anion-doping could shift the VB upwards and cause a narrowed bandgap of anatase. However, the above methods may have some disadvantages such as the VB upwards shifting could have a detrimental effect on the oxidation activity. Metal-ion dopants may become recombination centers for electrons and holes, which have a negative effect on the photocatalytic water-splitting reaction.¹⁸

In a previous study, combination of inorganic photocatalyst with hydrogenase coupled with MV as a redox mediator was studied. Efficiency of hydrogenase genetically formed in *E. coli* is 100 % to transferred electron and so total apparent quantum yield (AQY) of TiO₂/MV²⁺/hydrogenase in *E. coli* is higher than 30 % in presence of sacrificial agent of triethanolamine (TEOA). However, TiO₂ can be excited by only UV light (<350nm). Although high AQY is achieved, solar-to-hydrogen efficiency of photobiocatalytic system using TiO₂ as inorganic photocatalyst was reduced.²³

Dye-sensitizer anchored to anatase to improve the photocatalytic performance have attracted great attention in recent years. Dye could be excited upon visible light absorption and then excited electrons could transfer from the dye to the CB of anatase. As a result, dye-sensitized anatase can



be excited in the visible light region. Organic dyes are currently attracting much interest because of their active visible-light responses, flexible structures, economical and eco-friendly. Some organic dyes were examined for their light-harvesting capabilities and electron transfer properties such as perylene, cyanine, riboflavin, Eosin Y (hereafter referred to as EY) and so on.^{8,24–26} Among them, EY has been found to be an effective photosensitizer.^{30–31} Raman spectrum of bare anatase and EY adsorbed TiO₂ indicated that EY could effectively improve the intensity and the range of light absorption on anatase.²⁹ The EY-sensitized anatase also exhibited a high photo energy conversion efficiency. This is mainly because of the strong ester linkage formed between the carboxyl anchoring group of EY and anatase, which allows efficient electron injection from EY to anatase. However, this linkage was not stable in water due to hydrolysis and easily desorbed from TiO₂ and deactivated.^{8,30}

The anchoring group has been confirmed to influence the interaction between dye and substrate. Several experimental and theoretical studies reported that phosphonic acid was a potential alternative anchoring group.^{28–30} It had a strong binding interaction with anatase, showing better long-term stability. Compared to the carboxylic acid anchors, the most prominent benefit of phosphonic acid is the greater adsorption strength, whereas the electronic properties did not improve significantly. Pyridine group was found to be an efficient anchor for the charge injection from fluorescent dyes to anatase.³¹ The coordination bond between the pyridine ring and the Lewis acid site behaved as a unique intermolecular charge transfer media. Moreover, the pyridine ring exhibited high adsorption stability in water, enabling it to function effectively over extended periods in water-splitting systems. It is necessary to consider both the binding strength and the electronic properties of the anchoring group in order to design a high-performance water-splitting system. Thus, we proposed the use of a pyridine ring as an anchoring group in place of the



conventional carboxyl group to connect the EY and anatase. Since the position of the anchor attached to the molecule plays an important role in electron transfer, the isomer (ortho-, meta, para-) effect was considered in our theoretical study. The structures of the dye EY investigated in this work are illustrated in Figure 1. Comparative studies on the hybrid interfaces of anatase and Eosin Y with the different anchoring groups were performed by DFT and TD-DFT calculations. The geometries, binding interactions between dyes and anatase, electronic structures and electron transfer as well as the isomer effect on the dye / $\text{Ti}_{78}\text{O}_{160}\text{H}_8$ clusters were investigated and discussed. In addition, electron transport calculations were conducted by non-equilibrium Green's function at the DFT level of theory (NEGF-DFT) on the pyridine-based and the carboxyl-based molecular junction.

Synthesis of modified Eosin Y was performed by using bromobenzaldehyde and pyridin-4-ylboronic acid with catalytic amount of tetrakis(triphenylphosphine)palladium. Dye-sensitized TiO_2 (dye/ TiO_2) as photocatalytic material was prepared. Photocatalytic reduction of methyl viologen was performed to determine the light-absorbing capacity of photocatalytic materials. Photobiocatalytic H_2 production of dye/ TiO_2 coupled with *E. coli* was performed. Finally, we demonstrated the photobiocatalytic NH_3/H_2 production using dye/ TiO_2 coupled with cyanobacteria.

2. COMPUTATIONAL AND EXPERIMENTAL METHODS

2.1. Computational methods

Geometry optimizations of the isolated EY molecular structures shown in Figure 1 and their complexes with charge neutral $\text{Ti}_{78}\text{O}_{160}\text{H}_8$ cluster were performed by the DFT method with PBE exchange-correlation functional.³² Based on the optimized structures of dye / anatase, we studied



the binding energies (which was the difference between the total energy of dye / anatase, isolated dye and isolated anatase) and the optical properties of the six complexes, by performing TD-DFT calculations with hybrid B3LYP functional.^{33,34} Karlsruhe def2-SV(P)³⁵ basis set was applied for all atoms and N-1 Hay-Wadt³⁶ effective-core potential was employed for the titanium atoms. Based on this method, the optimized lattice properties of anatase crystal were $a=b=3.78 \text{ \AA}$ and $c=9.51 \text{ \AA}$, close to the experimental values of $a=b=3.79 \text{ \AA}$ and $c=9.51 \text{ \AA}$.³⁷ The band gap of anatase calculated periodic boundary condition (B3LYP functional and pob-TZVP basis set) was estimated to be 3.28 eV, which was in good agreement with the experimental values of 3.20 eV.^{38,39} All the dyes were adsorbed on the fivefold coordinated titanium atoms, which was the Lewis acid site with high reactivity.^{33,40} The above calculations were implemented in the Turbomole 7.7 program.

41



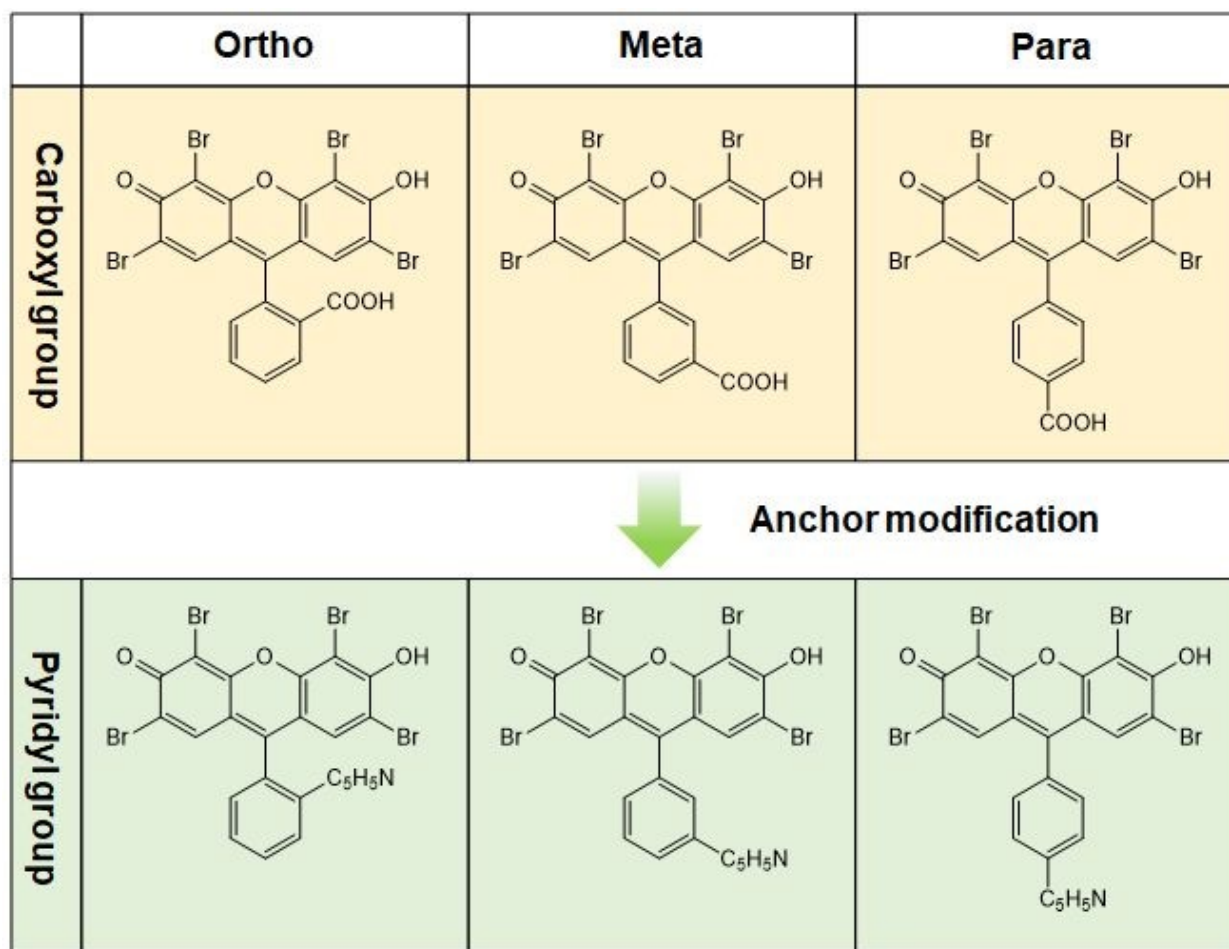


Figure 1. Molecular structures of the investigated Eosin Y isomers anchored with the conventional carboxyl group and modified pyridine group.



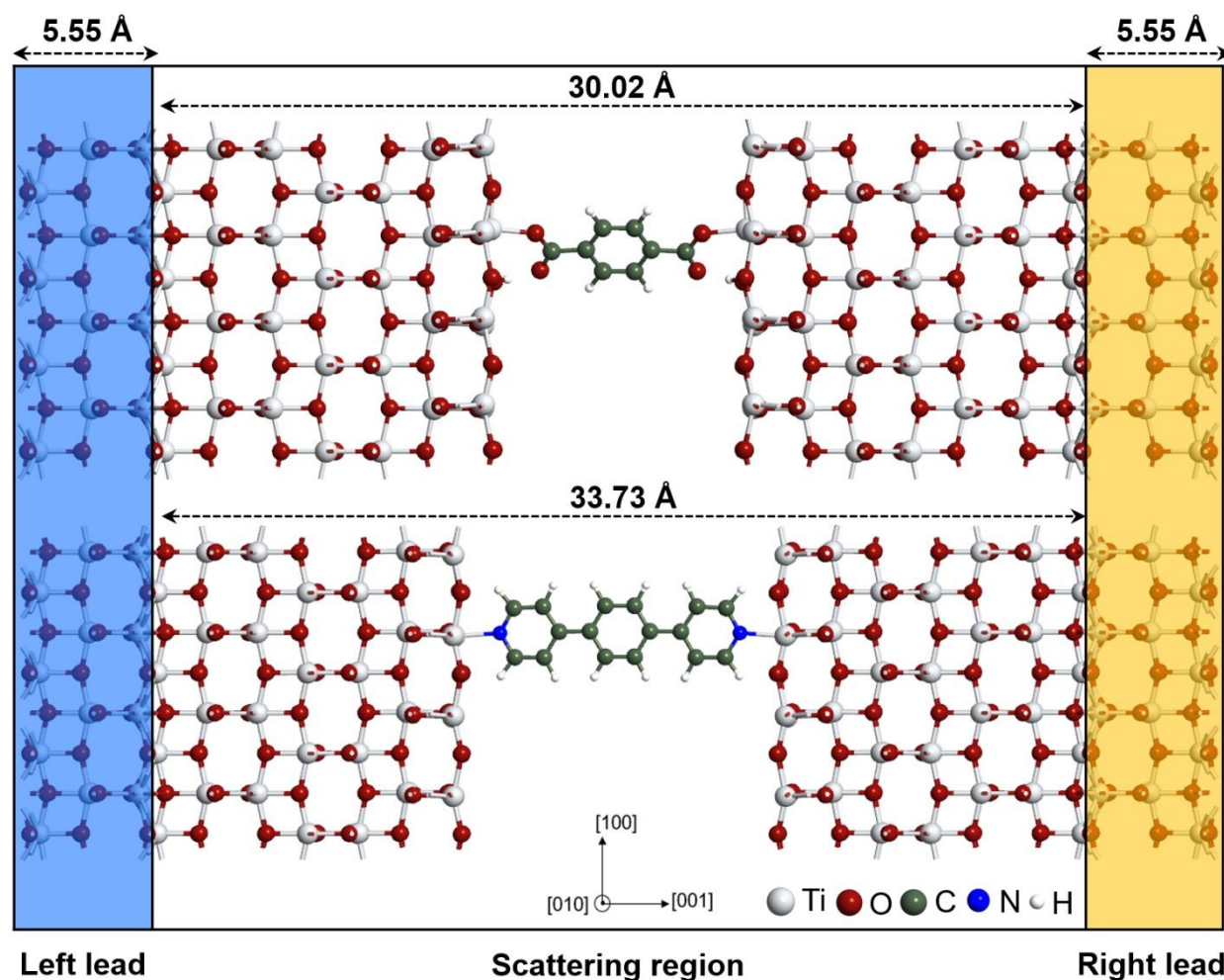


Figure 2. Structures of the carboxyl-linked device (upper panel) and the pyridine-linked device (lower panel). In all systems, the symmetrical electrodes had a length of 5.55 Å, while the length of the central region in the carboxyl-linked device and the pyridine-linked device was 30.02 Å and 33.73 Å, respectively.

To elucidate the mechanism of enhanced photocatalytic activity of the anatase / EY-pyridine, electron transport calculations were performed by the NEGF-DFT method,⁴² implemented in the QuantumATK package.⁴³ Local density approximation (LDA)⁴⁴ with the FHI⁴⁵ pseudopotential was employed for the calculations. A single zeta-polarized basis set was chosen for the titanium



atoms and a double zeta-polarized basis set was chosen for the other atoms.⁴⁶ The electric current and transmission spectra at the carboxyl-linked molecular junction and the carboxyl-linked molecular junction, as shown in Figure 2, were quantitatively investigated in this work. The electrode was modelled by the optimized anatase (001) - (4 × 4) surface with one O-Ti-O layer. For the central scattering region, it was composed of the investigated anchoring group (i.e., carboxyl group and pyridine group), benzene and three layers from each (i.e., three O-Ti-O layers). We used the simplest aromatic hydrocarbon benzene ring as the connection medium to investigate the electric transport through anatase and the different anchors. During the calculations, only the two top O-Ti-O layers as well as the investigated molecules in the scattering region were relaxed, while the two layers on each side in the scattering region and the two electrodes were frozen.

2.2. Synthesis of modified Eosin-Y (EY)

Synthesis of modified Eosin Y was performed by using bromobenzaldehyde and pyridin-4-ylboronic acid with catalytic amount of tetrakis(triphenylphosphine)palladium gave corresponding (pyridin-4-yl)benzaldehyde in 64-94% yields. The obtained products were reacted with resorcinol in methanesulfonic acid to give fluorescein type derivatives. These obtained compounds were reacted with excess amount of bromine in ethanol. The precipitated red colored powders were corrected to give corresponding modified Eosin Y in 36-42% yields. Thus, obtained modified products were analysis with ¹HNMR to confirm the objected product obtained. Details of synthesis method were mentioned in support information. From ¹HNMR analyses, the obtained final product is high purity and no bi-product was contained. The ¹HNMR was recorded with a Bruker AV600 (600 MHz) or a Bruker Avance 400 III HD (400 MHz) spectrometers. The ¹H NMR chemical shifts were reported to be δ values (ppm) relative to Me₄Si. The absorption spectra were



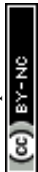
recorded on a Shimadzu UV-3600. All the solvents and reagents were of reagent quality, purchased commercially, and used without further purification.

2.3. Photocatalytic activity measurement

Photocatalytic reduction of methyl viologen aims to determine the light-absorbing capacity of photocatalytic materials. In principle, photocatalysts can absorb light energy and transfer photoexcited electrons to methyl viologen (MV) as an electron acceptor, facilitating the reduction of oxidized MV^{2+} to reduced $MV^{\bullet+}$. Therefore, measuring the amount of reduced $MV^{\bullet+}$ formed in the reaction directly indicates the capacity of the photocatalysts.

In this work, dye-sensitized TiO_2 (dye/ TiO_2) as photocatalytic material was prepared as follows. The hydrothermal grafting of dye onto the surface of TiO_2 nanoparticles was conducted without any coupling reagents.⁴⁷ First, 12.5 mmol of TiO_2 powder (1 g) was dispersed in 60 mL of H_2O using ultrasonication for 5 min, followed by stirring for 30 min to form a homogeneous slurry. Next, 7.5 μ mol of dye (approximately 5 mg) was added, and the mixture was stirred for 2 h in the dark to create a dye/ TiO_2 suspension. The resulting suspension was then transferred to a Teflon-lined autoclave and heat-treated at 160°C for 8 h. After cooling to room temperature, the product was collected by centrifugation at $10,000 \times g$ for 5 min, thoroughly washed with deionized distilled water to remove any unabsorbed dye molecules and dried at 100°C under vacuum to obtain dye/ TiO_2 nanoparticles.

To determine the visible light-absorbing capacity of dye/ TiO_2 nanoparticles, the reaction mixture comprised 100 mM L-cysteine pH 6-8, 1 mg/mL photocatalyst, and 5 mM methyl viologen (MV^{2+}) solution, with a total reaction volume of 3 mL in a 10 mm \times 10 mm quartz cuvette with a screw cap and a polytetrafluoroethylene/silicone septum. Oxygen was displaced by



bubbling nitrogen gas through the solution for 2 min. The reaction was initiated by irradiation under visible light using a 300-W Xenon lamp (MAX-303, Asahi Spectra, Japan) equipped with a 520 nm bandpass filter (XBPA520, Asahi Spectra, Japan). At each time point during the reaction, the cuvette was centrifuged at $1,000 \times g$ for 1 min to precipitate the particles that might interfere absorbance measurements. The reduced MV^{+} formed during the photocatalytic reaction of dye/ TiO_2 was monitored using a UV-Vis spectrophotometer (SH-1000Lab, Corona Electric Co., Ltd., Japan) and quantified using a molar absorption coefficient (ϵ) of $1.3 \times 10^4 \text{ M}^{-1} \text{ cm}^{-1}$, based on the absorbance value at 605 nm.^{48,49} AQY analysis for photocatalytic MV^{+} reduction is defined as shown below:⁵⁰

$$\text{AQY (\%)} = 100 \times \frac{\text{Rate of reduced } MV^{+} \text{ (mol}\cdot\text{s}^{-1}\text{)}}{\text{Rate of incident photon (mol}\cdot\text{s}^{-1}\text{)}}$$

Where light intensity at 520 nm is 0.013 W/cm^2 , irradiation area is 1 cm^2 , Avogadro's number is $6.022 \times 10^{23} \text{ mol}^{-1}$, rate of incident photon is $0.0562 \times 10^{-6} \text{ mol/s}$.

2.4. Photobiocatalytic H_2 production of dye/ TiO_2 coupled with *E. coli*

The combination of photocatalyst and biocatalyst was carried out according to our previous report⁴⁸ with slight modifications for H_2 production. The reaction solution consisted of 100 mM L-cysteine pH 8, 3 mg/mL dye/ TiO_2 composite, 5 mM MV^{2+} and 5 mg/mL recombinant *E. coli* in a quartz reactor with a total volume of 30 mL under anaerobic condition. After connecting the reactor to a closed gas circulation system linked to a gas chromatograph, the air in the reactor was evacuated and replaced with argon. The reaction was then initiated by irradiation with visible light through a 300-W Xenon lamp equipped with a 520 nm bandpass filter. At each time point, H_2 produced were sampled directly using argon as a carrier gas and monitored by a gas chromatograph (GC-8A, Shimadzu Corp., Japan) equipped with a molecular sieve 5 A column (GL Sciences Inc.,



Japan), a thermal conductivity detector at an oven temperature of 50 °C and an integrator (C-R6A, Shimadzu Corp.). AQY analysis of H₂ production is calculated as shown below:

$$\text{AQY of H}_2 (\%) = 100 \times \frac{2 \times \text{Rate of H}_2 \text{ production (mol}\cdot\text{s}^{-1})}{\text{Rate of incident photon (mol}\cdot\text{s}^{-1})}$$

Where light intensity at 520 nm is 0.013 W/cm², irradiation area is 1 cm², Avogadro's number is $6.022 \times 10^{23} \text{ mol}^{-1}$, rate of incident photon is $0.0562 \times 10^{-6} \text{ mol/s}$.

2.5. Photobiocatalytic NH₃/H₂ production using dye/TiO₂ coupled with cyanobacteria

The combination of photocatalysts and biocatalysts was performed based on our previous report⁴⁹, with slight modifications. Cyanobacterium *Anabaena variabilis* ATCC 29413 was utilized in this study. Cyanobacterial cells were aerobically cultivated in Allen & Arnon medium supplemented with 20 μM Na₂MoO₄ to promote heterocyst differentiation under the light intensity of 5,000 Lux (68 μmol/m²/s) at 26 °C and 140 rpm shaking incubator. At a cell density of 1.0 at A₆₈₃ and chlorophyll a (Chl a) content of ~12 μg/mL, the cells were harvested by centrifugation at 10,000 × g for 5 min for experiments. The reaction solution consisted of 100 mM L-cysteine pH 7, 2 mg/mL of dye/TiO₂ composite, 10 mM MV²⁺ and 50 mg/mL of cyanobacterial cell mass in a quartz reactor with a total volume of 100 mL under anaerobic condition. After connecting the reactor to a closed gas circulation system, the reaction was initiated by irradiating it with visible light from a 300-W xenon lamp equipped with a 520 nm bandpass filter.

At each time point, H₂ production and N₂ consumption were monitored using a gas chromatograph (GC-8A, Shimadzu Corp., Japan) equipped with a thermal conductivity detector and an integrator C-R6A (Shimadzu Corp.), with the oven temperature set at 50 °C. The reaction gas was passed through a molecular sieve 5A column (GL Sciences Inc., Japan) using argon as a carrier gas.⁴⁸ For NH₃ determination, samples were collected and filtrated using Amicon® Ultra-



15 Centrifugal Filters-10K (Merck Millipore) at $5,000 \times g$ for 1 h to remove insoluble components. A 1-mL filtrate was injected into a cation exchange chromatography (Dionex, USA) equipped with an IonPacTM CG12A (4×50 mm) guard column and an IonPac[®] CS12A (4×250 mm) analytical column^{49,51}. The concentration of NH_4^+ was calculated using a calibration curve prepared with standard NH_4Cl . AQY analysis of NH_3 production is calculated as shown below:

$$\text{AQY of } \text{NH}_3 (\%) = 100 \times \frac{3 \times \text{Rate of } \text{NH}_3 \text{ production (mol}\cdot\text{s}^{-1})}{\text{Rate of incident photon (mol}\cdot\text{s}^{-1})}$$

Where light intensity at 520 nm is 0.013 W/cm^2 , irradiation area is 1 cm^2 , Avogadro's number is $6.022 \times 10^{23} \text{ mol}^{-1}$, rate of incident photon is $0.0562 \times 10^{-6} \text{ mol/s}$.

3. RESULTS AND DISCUSSION

3.1. Computational design of Eosin Y (EY)

Optimized geometries of the EY isomers with the carboxyl and pyridine anchors shown in Figure 1 adsorbed on anatase nanoparticle are shown in Figure 3. Here we show the magnified views of the adsorption points of the molecules on anatase. Regarding the full structures of the investigated dyes on anatase, the Cartesian coordinates of the complexes can be found in Table S1 ~ Table S6, in the Supporting Information. EY isomers with the carboxyl anchoring group on the anatase particle were in the H-bonded monodentate adsorption mode with the H atom of the carboxyl group connected to the two-coordinated O atom on the anatase substrate, whereas the pyridine ring adsorbed on the anatase by a solely Ti-N bond. The length of the main electron transport path, Ti-O bond in the anatase / EY-carboxyl, was around 2.15 \AA , which was close to that reported previously between anatase and the dyes with the carboxylic acid group, indicating a strong binding interaction between the carboxyl group and anatase.^{52,53} This distance was not far from the Ti-N bond connected the pyridine ring and anatase (in the region of 2.26 \AA to 2.28 \AA). As



can be seen from the calculated binding energies in Figure 3, EY isomers anchored by the carboxyl group bind stronger than the corresponding isomers anchored by pyridine to the anatase nanoparticle. The total energies of the isolate dyes, isolate anatase and their combined systems are given in Table S7. On the other hand, the dihedral angles (from 82.05° to 84.93°) formed by the O and Ti atoms of EY-carboxyl / anatase were smaller than those of EY-pyridine / anatase. The smaller dihedral angle could maximize the interaction between adsorbate and substrate, thus contributing to the high binding energy.⁵⁴ Though the EY-pyridine isomers had weaker binding, they show the advantage in stabilization in water compared to the unstable carboxyl group in water due to hydrolysis.⁸

The frontier molecular orbitals of the EY anchored by the carboxyl group and pyridine group are displayed in Figure 4 and Figure 5, respectively. The highest occupied molecular orbitals (HOMOs) of all the dyes were delocalized over the three benzene rings and mainly consisted of 2p contributions of the C, Br, and O atoms of the EY.⁵⁴ The similar HOMO distributions imply that the modification of the anchoring group for the EY dye retained its molecular character. The lowest unoccupied molecular orbital (LUMO) contributions mainly came from the Ti atoms in the center of anatase nanoparticles. Furthermore, the LUMOs were spatially separated from the HOMOs, which could reduce the probability of electron-hole recombination upon photoexcitation.⁵⁵ Similar to the adsorption energy, the HOMO-LUMO gaps of the EY isomers anchored by the carboxyl group were smaller than the corresponding isomers anchored by the pyridine ring. All the linkage types were characterized with a narrow band gap (< 2.5 eV), in visible light absorption ranges.



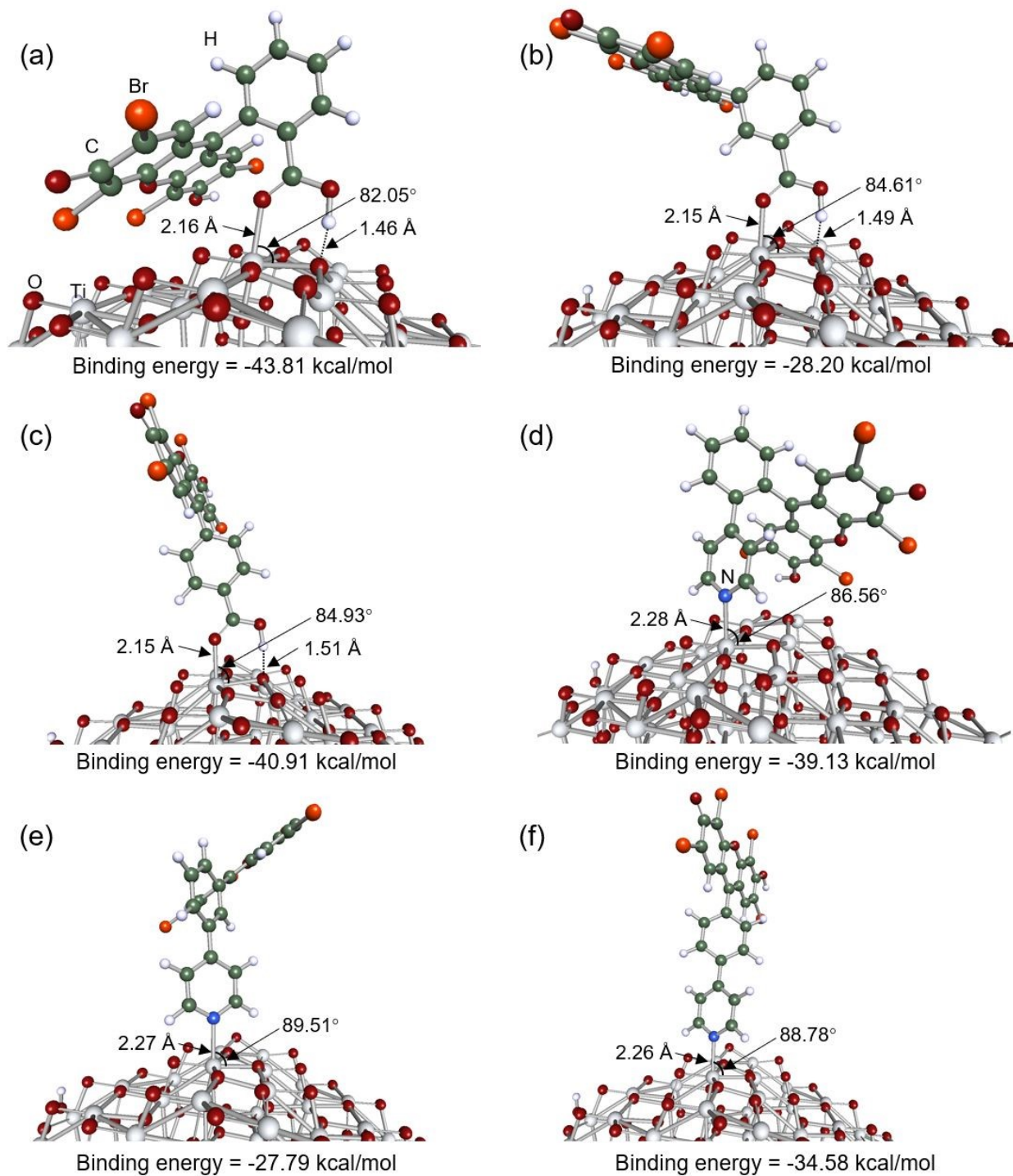


Figure 3. Optimized geometries and the binding energies of the Eosin Y isomers anchored by the carboxyl and pyridine group on anatase. (a) EY, (b) MEY, (c) PEY, (d) OPyE, (e) MPyE, and (f) PPyE.



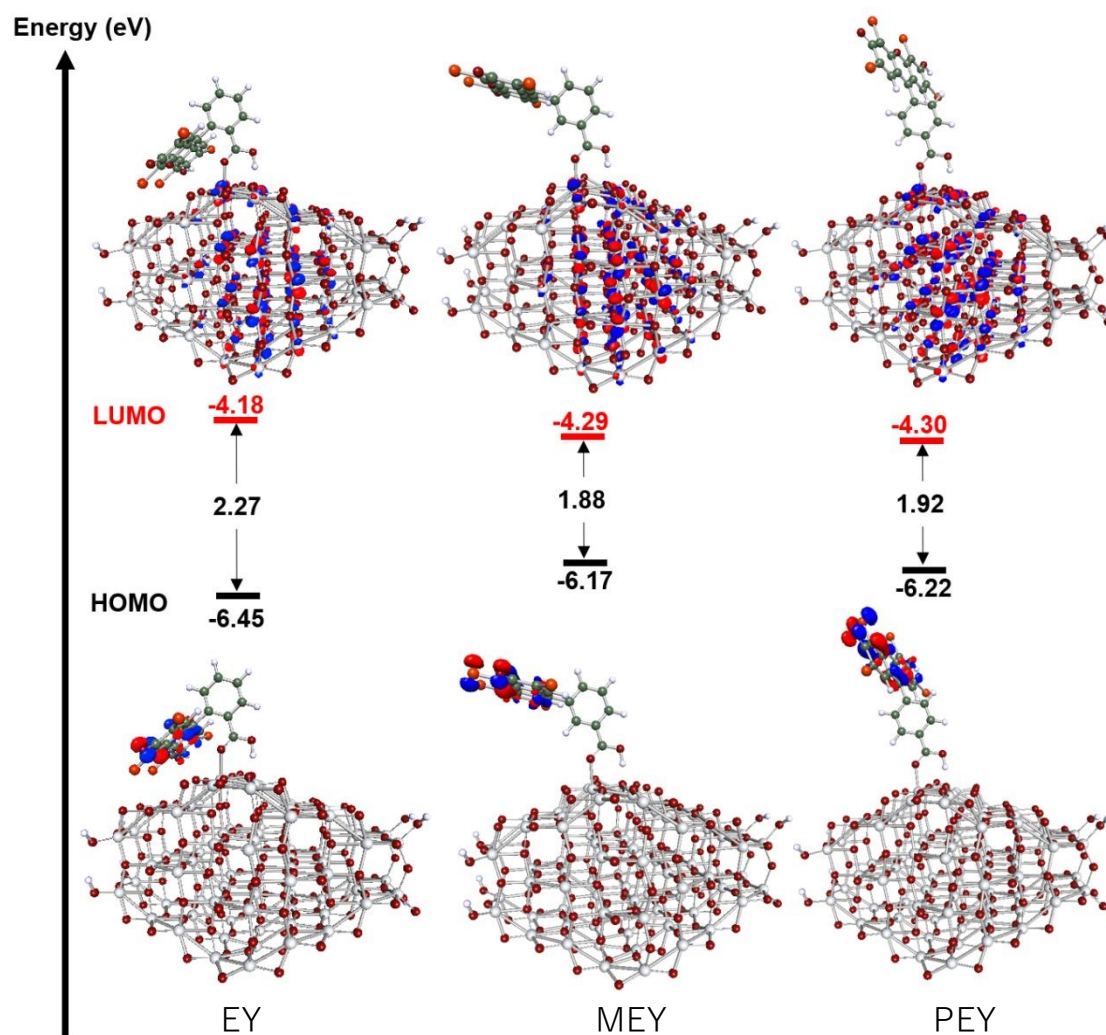


Figure 4. Frontier orbitals and energy levels of the HOMO and LUMO for the Eosin Y isomers anchored by the carboxyl group.



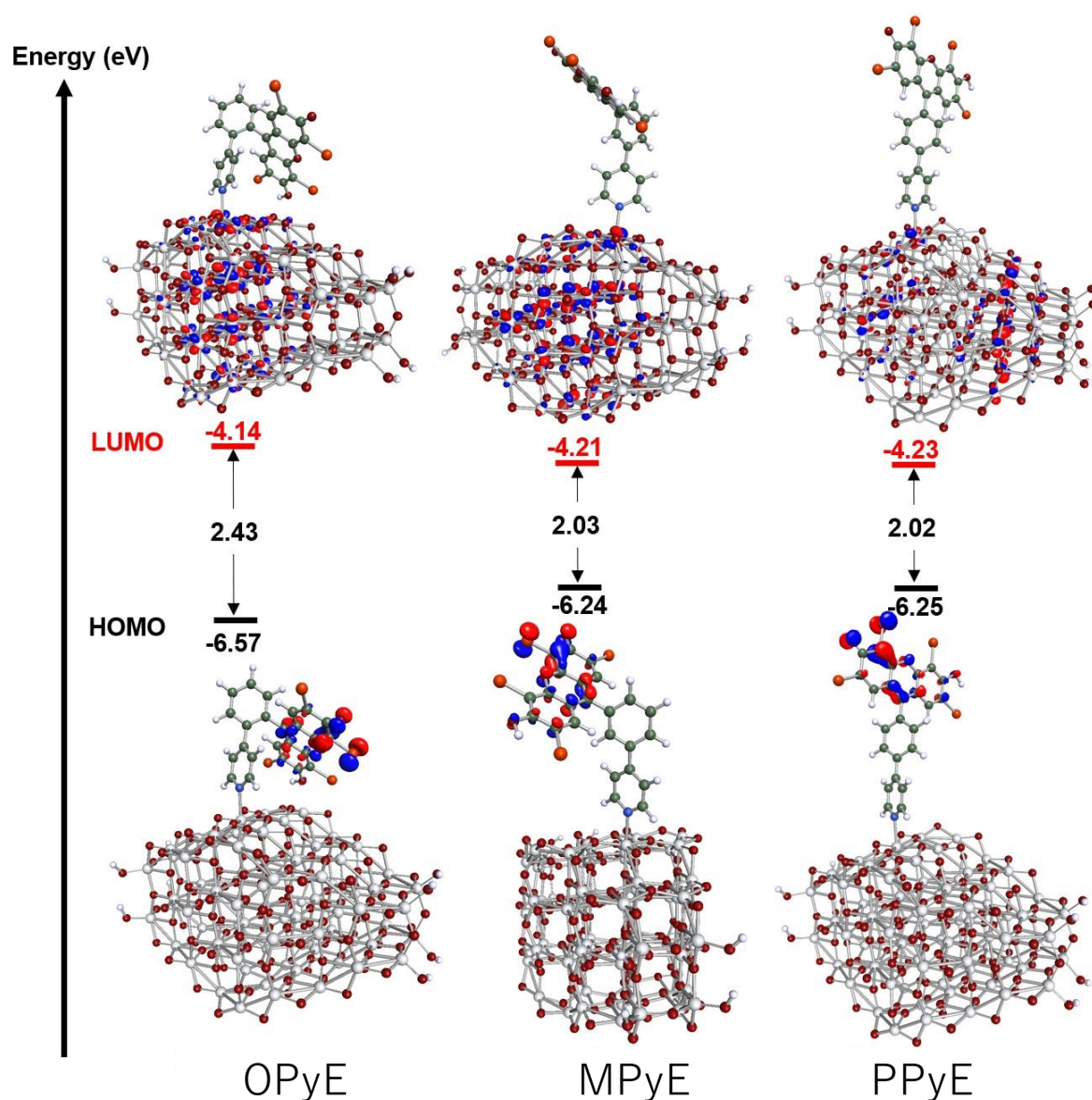


Figure 5. Frontier orbitals and energy levels of the HOMO and LUMO for the Eosin Y isomers anchored by the pyridine group.

Though all six forms could have visible adsorption and electron transfer from the dye to the particle, their UV-vis absorption spectra differed significantly. The wavelengths, oscillator strengths and assignments for the two most probable singlet excitation states are reported in Table



1. The main difference is in the oscillator strength for singlet excitations of the composites, with those linked by the pyridine ring showing the higher photoactivity, compared to those linked by the carboxyl group. The oscillator strength of the anatase sensitized by EY anchored by OPyE was the highest (4.76×10^{-2}) among the investigated complexes, which was 10 times higher than that anchored by PEY (4.44×10^{-3}). The higher transition probability indicates the stronger optical interaction of the designed EY with the anatase particle, as well as the intense transition corresponding to the HOMO \rightarrow LUMO+1 excitation. At the same time, Anatase / OPyE showed a significant advantage in green light absorption, ca. 520 nm, whereas a red-shift of the maximum absorption over the range of 606 nm to 655 nm was observed for anatase / PEY. It was worth noting that the difference between the binding energies of anatase / PEY and anatase / OPyE was only 1.78 kcal/mol. This slight destabilization caused by anchor modification could be masked by the non-negligible optically excited transition. In other words, anatase / OPyE presented unique features in binding interaction, stability in water, electron transfer and light absorption. In addition, there were two absorption peaks appeared at 571 nm and 615 nm in the combined system of anatase and PPyE, which were also stronger than those calculated for anatase / PEY. The intense absorption of visible light for the anatase / EY-pyridine will have a marked effect on its application in harvesting solar energy photocatalytic systems.

Table 1. Computed excitation properties of the combined systems of anatase and the Eosin Y isomers anchored by the carboxyl and pyridine group. The two most intense singlet excitation states are reported.

	Excited state	Wavelength (nm)	Oscillator Strength	Transition assignment ^a
Carboxyl-ortho (EY)	$S_0 \rightarrow S_1$	635.72	3.20×10^{-5}	H \rightarrow L (74%), H \rightarrow L+2 (15%)
	$S_0 \rightarrow S_5$	528.12	1.62×10^{-5}	H \rightarrow L+8 (33%), H \rightarrow L+6 (18%)
Carboxyl-meta (MEY)	$S_0 \rightarrow S_4$	626.24	4.28×10^{-4}	H \rightarrow L+3 (81%)
	$S_0 \rightarrow S_1$	736.38	1.78×10^{-4}	H \rightarrow L (95%)
Carboxyl-para (PEY)	$S_0 \rightarrow S_4$	605.68	4.44×10^{-3}	H \rightarrow L+1 (96%)
	$S_0 \rightarrow S_2$	655.19	1.16×10^{-3}	H \rightarrow L+3 (92%)
Pyridine-ortho (OPyE)	$S_0 \rightarrow S_3$	523.67	4.76×10^{-2}	H \rightarrow L+1 (42%), H \rightarrow L+3 (40%)
	$S_0 \rightarrow S_2$	530.39	4.58×10^{-2}	H \rightarrow L+1 (50%), H \rightarrow L+3 (28%)
Pyridine-meta (MPyE)	$S_0 \rightarrow S_4$	574.62	4.77×10^{-4}	H \rightarrow L+3 (95%)
	$S_0 \rightarrow S_2$	619.14	1.24×10^{-4}	H \rightarrow L+1 (97%)
Pyridine-para (PPyE)	$S_0 \rightarrow S_4$	571.11	8.05×10^{-3}	H \rightarrow L+3 (95%)
	$S_0 \rightarrow S_2$	614.73	1.89×10^{-3}	H \rightarrow L+1 (98%)

^a Contributions over 15% are displayed. H and L refer to HOMO and LUMO, respectively.

The above results elucidate that modifying the anchoring group to the pyridine ring could significantly improve the photocatalytic performance of anatase. To further understand the electron transfer by the pyridine ring, we examined the electric current in the carboxyl-linked device and the pyridine-linked device, respectively. In the plotted I - V curves in Figure 6a and b, the current increased with the increasing bias voltage for the two devices. Particularly, the current increased sharply at the voltage of 1.6 V, where the current in the carboxyl-linked molecular junction was over three orders of magnitude lower than that in the pyridine-linked one. The transmission spectra at 1.6 V bias for the two investigated devices are given in Figure 6c and d.



Both transmission spectra were characterized by the sharp peak above the Fermi level, which originated from the LUMO of the molecules. In the case of the pyridine-based device, two peaks appeared among the bias window of $[-0.8 : 0.8]$ eV at 1.6 V. This indicated that LUMO served as a conducting channel when the pyridine ring connected to the anatase. Meanwhile, the calculated energy level of the LUMOs for the combined systems of anatase and EY anchored by pyridine (PyE) in Figure 5 were closer to Fermi energy compared to the HOMO energy. Thus, it further confirmed that LUMO dominated the electron transport through the pyridine-connected junction.

⁵⁶ This was in line with the lower energy positions of LUMOs for the pyridine-linked anatase and EY compared to anatase / EY-carboxyl. The intense resonance tunneling at high applied biases through the LUMO channel contributed significantly to the high current of the pyridine-based device. The occurrence of the similar electron injection mechanism was found in other pyridine-linked molecular junctions, such as pyridine bridged between two Ag, Au and graphene nanoribbon ⁵⁷⁻⁵⁹, based on experimental and theoretical studies. The implications of the photocatalytic performance for the pyridine-anchored EY-sensitized anatase are under continuous experimental investigation. Our work provides a design of EY with a pyridine ring to maximize the electron injection. We performed Mulliken population analysis of representative EY/TiO₂ complexes to quantify interfacial charge redistribution. The results are consistent with our conclusions on electron distribution and interface charge dynamics. In case of MPyE, it donates ~ 0.29 e⁻ to the Ti₇₈O₁₆₀H₈ cluster, whereas OPyE donates ~ 0.47 e⁻, leading to the higher charge-transfer ability of OPyE.



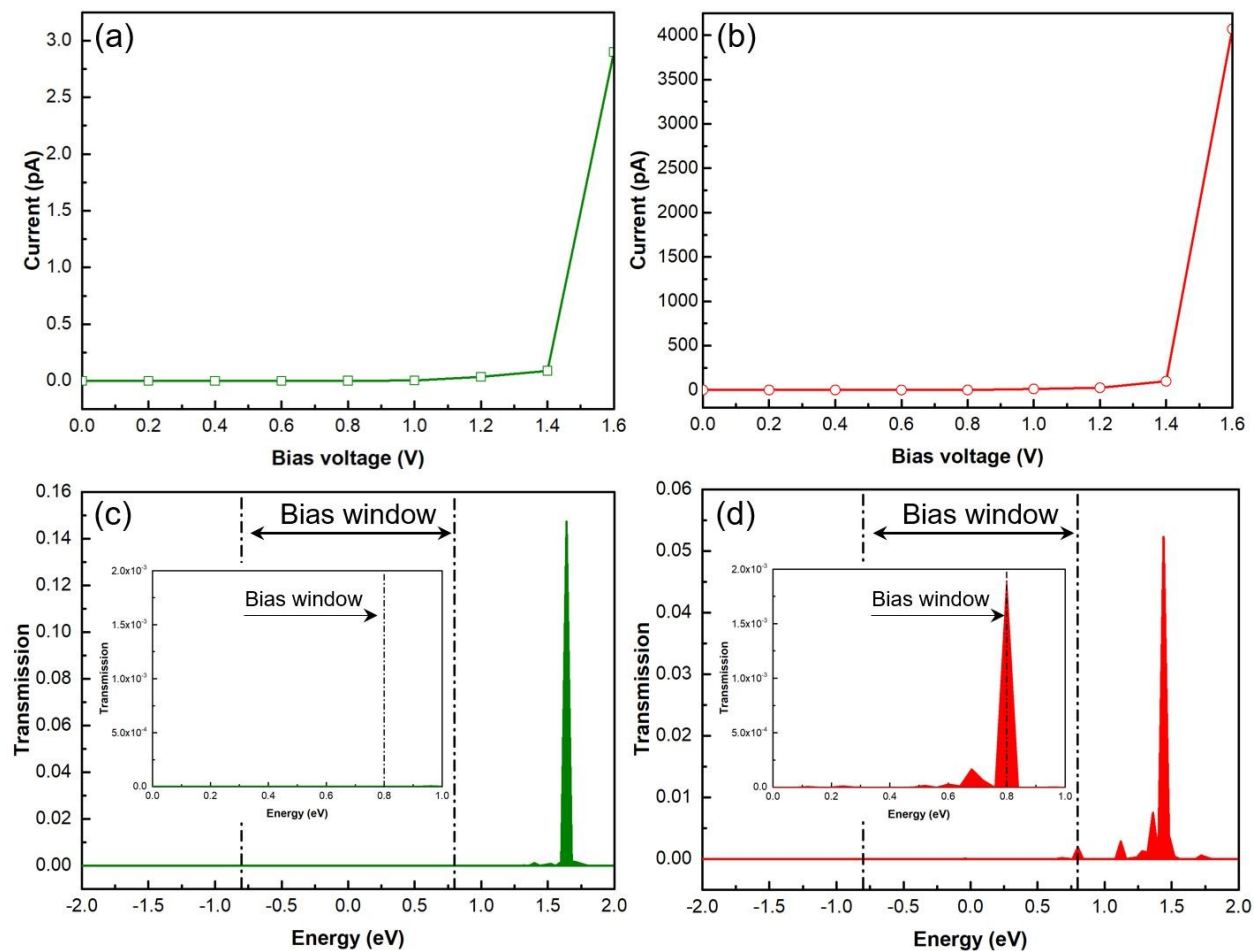


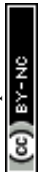
Figure 6. I - V curves of (a) the carboxyl-based device as well as (b) the pyridine-based device, and the transmission spectra of (a) the carboxyl-based device as well as (b) the pyridine-based device at 1.6 V bias, where the insets show the magnified spectra around the bias window.



3.2. Photo spectroscopic characterization of Eosin Y (EY) on TiO₂

To validate the theoretical calculation suggestions, experimental measurements for the charge transfer from surface modified Eosin Y (EY) to TiO₂ was conducted. Figure 7 shows UV-Vis absorption spectra of organic dye/TiO₂. Strong absorption peak was observed around 550 nm on all EY modified TiO₂ and this absorption peak is typical peak to EY. On the other hand, modification of EY shows peaks shift depending on the modified functional group and position. Comparing to the pristine EY, carboxyl modified EY shows higher wavenumber of absorption peak suggesting strong electronic interaction with TiO₂, which is also suggested by DFT calculation. Since the absorbance of peak around 520 nm was weak on QPyE, MPyE, PPyE modified TiO₂ comparing with carboxyl EY. This suggests molecular photoexcitation coefficient seems to be small on pyridine modified EY. Figure S1 shows photographs of dye modified TiO₂ and Figure S1 shows photographs of dye modified TiO₂. Almost the same color, however, in agreement with UV-Vis, pyridine modified TiO₂ shows red color. Figure S2 shows 1M aqueous solution of modified EY and UV-Vis of 1M aqueous solution of modified EY and almost the same order of absorbance with that on TiO₂ shown in Figure 7a was observed. So, molecular excitation coefficient is changing by modified group and PyE is generally small molecular excitation coefficient. This could be explained by expanding the conjugation length by pyridine group.

Photoluminescence spectra is effective for analysis of annealing efficiency of photoexcited charge. Photoexcited charge is generally recombined with hole and electron formed, and recombination of charge forms photoluminescence or heat. As shown in Figure 7b, broad



photoluminescence peak was observed around 600 nm on pristine EY modified TiO₂. On the other hand, the peak intensity was decreased as the following order OPyE>MPyE>PPyE>MEY>PEY>EY. This peak intensity represents the charge transfer efficiency and weaker intensity suggests photoexcited charge is transferred to conduction band of TiO₂ with more efficiently. Since molecular excitation efficiency was changed, normalized photoluminescence (PL) intensity by UV-Vis absorbance was shown in Table S8. Normalized PL intensity was as follows; MPyE>OPyE=EY>PEY>PPyE>MEY, demonstrating that the charge transfer occurs easier on PPyE and MEY which is suggested by theoretical calculation.

Life of photoexcited charge was further studied by transient photoluminescence spectra (Figure S3 and Table S9 in the Supporting Information). Time dependence of photoluminescence decay period is varied with modified group and its position. In agreement with the order of PL peak intensity shown in Figure 7b, PL decay period is also longer. The estimated decay rate on each EY modified TiO₂ is also summarized in Table 2. Since fast backward reaction shows fast decay of PL, longer PL on pyridine modified EY ($\tau = 3.03 - 3.59$ ns) suggests photoexcited charge has long life which means photoexcited electron can transfer to TiO₂ conduction band and charge was separated state. This long life of photoexcited electron may be effectively transfer to the active site to photocatalytic reaction. As predicted by theoretical calculation, para-modified pyridine EY shows the fast charge transfer to TiO₂.



Table 2 Spectrophotometric measurements of Eosin Y and its derivatives.

Dye/TiO ₂	EY	MEY	PEY	OPyE	MPyE	PPyE
λ_{max} (nm)	527	539	537	544	535	537
Abs (a.u.)	0.83	0.85	0.87	0.29	0.18	0.26
ϵ (Lmol ⁻¹ cm ⁻¹)	88,000	79,500	86,350	29,110	17,500	26,490

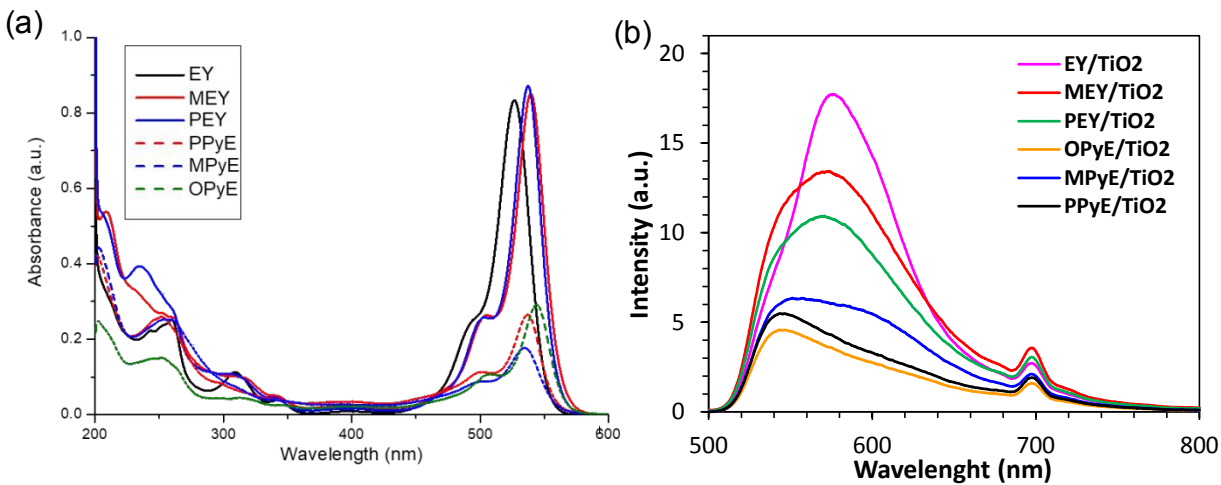


Figure 7 (a) UV-Vis and (b) photoluminescence spectra of dye/TiO₂ nanoparticles.

3.2. Photocatalytic reduction of methyl viologen

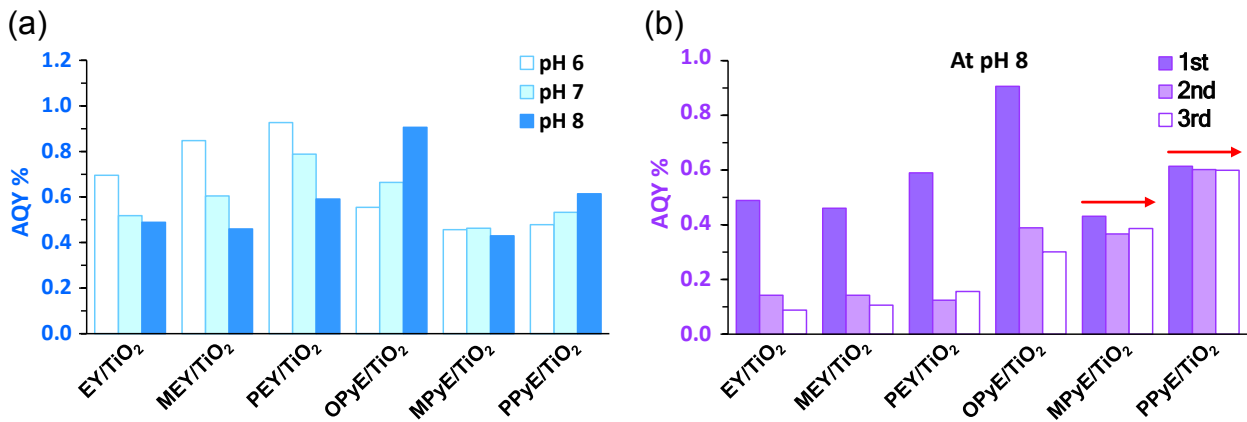
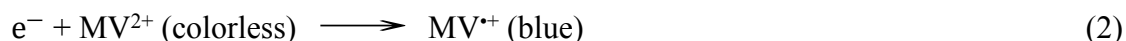
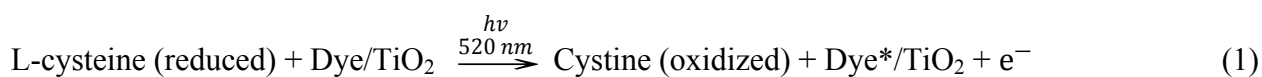


Figure 8 Methyl viologen ($MV^{•+}$) reduction of different dye/ TiO_2 nanoparticles. (a) Effect of pH on $MV^{•+}$ reduction and (b) stability of the nanoparticles in the reaction solution determined by testing their reusability up to three times. The raw data are shown in Figure S4 and Figure S5.

$MV^{•+}$ reduction experiment was performed to demonstrate the transport property of photoexcited electrons generated by photocatalysts under light illumination. In the photocatalytic $MV^{•+}$ reduction by dye/ TiO_2 nanoparticles, L-cysteine was employed as a sacrificial electron donor, dye/ TiO_2 composites served as the photocatalytic material, and oxidized methyl viologen (colorless MV^{2+}) acted as an electron acceptor, with its reduced form (dark blue $MV^{•+}$) detectable by spectrophotometry. It was found that no $MV^{•+}$ reduction activity occurred with pure TiO_2 , indicating that pure TiO_2 cannot absorb visible light energy to excite electrons. In contrast, the formation of reduced $MV^{•+}$ occurs in the presence of dye on the TiO_2 surface, implying that eosin and its derivatives can absorb light energy at 520 nm to excite electrons to the LUMO level while simultaneously receiving electrons from L-cysteine at the HOMO level. The reaction mechanism of photocatalytic MV^{2+} reduction by Dye/ TiO_2 in this system can be proposed as follows:



In general, several factors can affect the performance of photocatalyst that should be studied. As shown in Figure 8a, the effect of pH reveals that carboxyl-eosin/ TiO_2 composites exhibit higher activity under acidic conditions, while pyridine-eosin/ TiO_2 composites perform better under alkaline conditions. This work reveals the range of optimal pH for each dye/ TiO_2 nanoparticle in practical applications. In addition to the pH effect, stability is another key factor to consider. Generally, pure dye molecules dissolved in the reaction solution cannot be reused after experiments. Therefore, dyes anchored on TiO_2 surface known as dye/ TiO_2 composites have



been developed to improve their reusability or more strong bonding. In this study, the reusability of dye/TiO₂ nanoparticles was evaluated based on MV^{•+} reduction activities at pH 8. Each dye/TiO₂ nanoparticle was reused three times for the reaction as shown in Figure 8b. Among the different photocatalysts, AQY analysis clearly shows that only MPyE/TiO₂ and PPyE/TiO₂ remain stable after three reuse cycles, while the efficiency of other dye/TiO₂ photocatalysts decreased by more than 50%. It is known that dyes bound to the hydroxy site of titanium dioxide by dye-carboxy groups are easily desorbed by hydrolysis in the presence of water.^{60,61} Although computer modeling suggests that both carboxyl and pyridine eosin could bind on TiO₂, the experimental results indicate that only MPyE and PPyE are stable on TiO₂ surface in our reaction system. Although reasonable high photoexcited property was achieved on EY without modification, decrease in activity with time is the most serious drawback, however, MPyE and PPyE shows no degradation during cycle uses. So, in addition to the high efficiency, high stability was achieved by strong bonding of pyridine group of MPyE and PPyE to TiO₂. Therefore, pyridine-meta and pyridine-para eosin are the most suitable candidates for further development in future studies.

3.3. Dye-modified TiO₂ in photobiocatalytic H₂ production

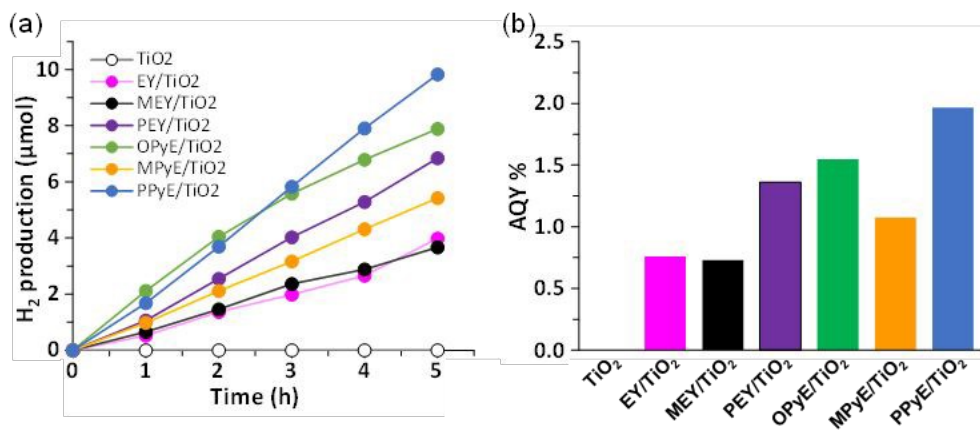


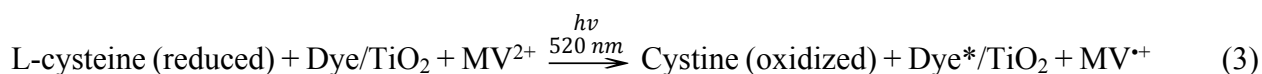
Figure 9 Photobiocatalytic H₂ production of dye/TiO₂ composite coupled with recombinant *E. coli* expressing [FeFe]-hydrogenase. (a) A time-course and (b) AQY analysis of H₂ production



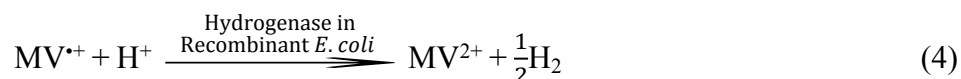
obtained from the reaction mixture including 100 mM L-cysteine pH 8, 3 mg/mL of dye/TiO₂ composite, 5 mM MV²⁺ and 5 mg/mL cell mass of recombinant *E. coli* under visible light illumination at 520 nm.

To demonstrate the usability of EY modified anatase photocatalytic for H₂ production, we typically combined with a biocatalytic enzyme, hydrogenase, in photobiocatalytic process. In our system, each dye/TiO₂ nanoparticle serves as a photocatalyst, while hydrogenase-expressing bacterial cell acts as a biocatalyst in the presence of L-cysteine solution as a sacrificial electron donor and MV²⁺ as an electron mediator that transfers photoexcited electrons from the photocatalyst to the biocatalyst for H₂ production.⁵⁰ The mechanism of the photobiocatalytic system in this work is illustrated below:

Photocatalytic reaction (light reaction):



Biocatalytic reaction (dark reaction):



According to the results shown in Figure 9, all dye/TiO₂ composites can be utilized visible light in the photobiocatalytic system when coupled with hydrogenase-expressing recombinant *E. coli* for H₂ production (Figure 9a). Among the five different photocatalysts, PPyE/TiO₂ demonstrated the highest activity, achieving an AQY of 1.97%, followed by OPyE/TiO₂, PEY/TiO₂, MPEY/TiO₂, EY/TiO₂, and MEY/TiO₂, respectively (Figure 9b) under addition of sacrificial agent. In general, pyridine-eosin/TiO₂ composites exhibit higher efficiency than carboxyl-eosin/TiO₂ composites corresponding to their photocatalytic reduction of MV²⁺, while pure TiO₂ cannot absorb light energy at 520 nm for H₂ production. This indicates that dye-sensitized molecules on the surface of TiO₂ can absorb visible light energy at 520 nm, generating and transferring photoexcited electrons



to the biocatalytic reaction in recombinant *E. coli* for H₂ production. In according with prediction, this high AQY was assigned to the efficient charge injection of electron from dye to conduction band of TiO₂. This could be related with expanded π conjugated orbital.

3.4. Dye-modified TiO₂ in photobiocatalytic NH₃ production

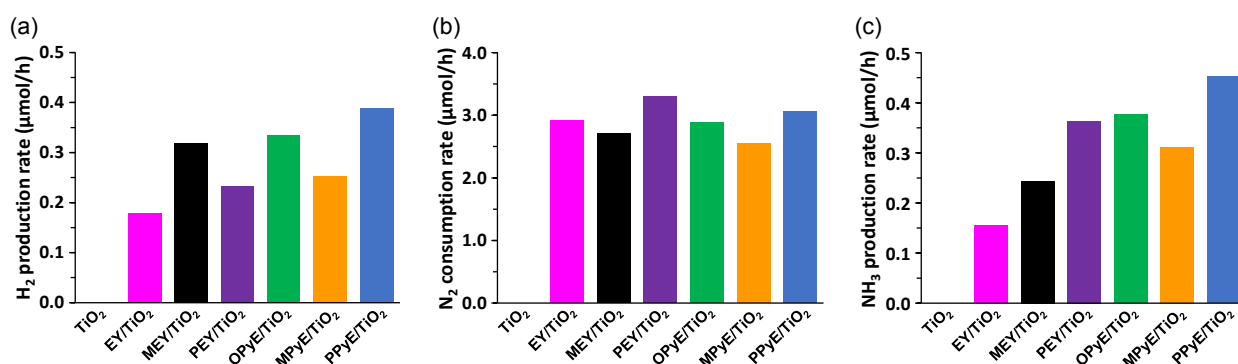
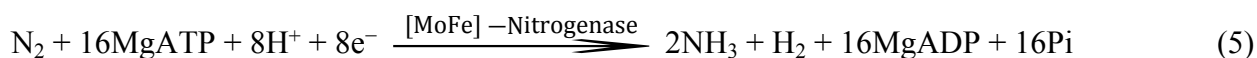


Figure 10 Rate of (a) H₂ production, (b) N₂ consumption and (c) NH₃ production produced from photobiocatalytic system of dye/TiO₂ coupled with cyanobacteria in the reaction system including 100 mM L-cysteine pH 7, 2 mg/mL dye/TiO₂, 10 mM MV²⁺ and 50 mg/mL cyanobacterial cell mass under visible light illumination at 520 nm. The raw data are also shown in Figure S6 and AQY analysis in Table S10.

In nature, the ability to synthesize NH₃ is observed in various species of bacteria, archaea, and cyanobacteria under ambient conditions. Nitrogenase is the only biocatalytic enzyme capable of fixing nitrogen by breaking the strong N≡N triple bond of dinitrogen (N₂) gas to NH₃, as shown in Equation (5):⁶²



Although N₂-fixing microorganisms can produce extracellular NH₃ without generating greenhouse gases or requiring high energy input, nitrogen metabolism in these organisms is tightly regulated to maintain intracellular C-N balance and amino acid pool homeostasis.⁶³ Due to the



low productivity of natural NH_3 synthesis through nitrogenase activity and ATP-dependent photosystem I, the replacement of the photosystem with photocatalysts is the focus of this study.

In the filamentous cyanobacterium *A. variabilis*, nitrogenase is naturally expressed from the *nif* gene cluster within differentiated heterocysts, which function as specialized sites for N_2 reduction.⁶⁴ Notably, it has been reported that methyl viologen (MV^{2+}), as an electron mediator, can transfer electrons to nitrogenase, mimicking the natural electron flow through the P-cluster to FeMoco at the enzyme's active site.^{65,66} This finding suggests the feasibility of developing an artificial photobiocatalytic system to enhance NH_3 production efficiency under mild conditions.

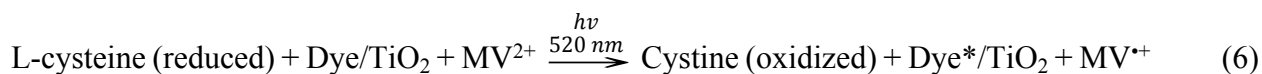
In this study, dye-modified TiO_2 was applied in a photobiocatalytic system coupled with cyanobacteria *A. variabilis* for NH_3 production in the presence of MV^{2+} and a sacrificial electron donor under visible light (520 nm). During the reaction, the kinetics of H_2 production and N_2 consumption were simultaneously monitored, as shown in Figure S6 (Supporting Information). The rates of NH_3 production, H_2 production, and N_2 consumption are presented in Figure 10. Among the different dye/ TiO_2 composites tested, pyridine-EY/ TiO_2 (particularly PPyE/ TiO_2 and OPyE/ TiO_2) demonstrated higher efficiency in this system, with superior rates and AQY compared to carboxyl-EY/ TiO_2 , as shown in Table S10 (Supporting Information). However, no significant differences were observed in the rates of N_2 consumption.

The results demonstrate that L-cysteine acts as an effective sacrificial reagent, donating electrons to deplete the HOMO level of dye/ TiO_2 particles. The excited electrons are transferred to MV^{2+} , reducing it to $\text{MV}^{•+}$ during the photocatalytic reaction, which proceeds similarly to the light reaction of H_2 production described in Equation (3). The simultaneous production of NH_3 and H_2 , along with N_2 consumption, indicates that the reduced $\text{MV}^{•+}$ molecules serve as electron mediators, transferring electrons to cyanobacterial nitrogenase for N_2 reduction and NH_3/H_2

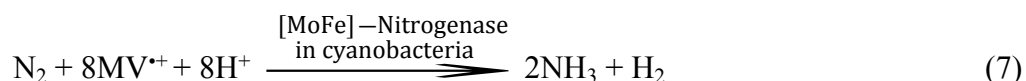


generation under visible light (520 nm). The proposed reaction mechanism for artificial photobiocatalytic NH_3 production using dye/ TiO_2 and cyanobacteria is outlined below:

Photocatalytic reaction (light reaction):



Biocatalytic reaction (dark reaction):



4. CONCLUSION

This study explored the possibility of improving the photocatalytic performance of EY / anatase TiO_2 by anchoring modification. Pyridine ring was used to replace the conventional carboxyl group linker. The structures, adsorption strengths, and electron transfer properties for the systems of anatase and EY anchored by the carboxyl and pyridine ring position were investigated through DFT and TD-DFT calculations and confirmed with experimental support. The adsorption of EY with the carboxyl acid was found to be much stronger than that with the pyridine ring, irrespective of the anchor positions (ortho, para, meta). While pyridine-linked EY and anatase showed prominent optical properties, the calculated oscillator strength of anatase / EY with pyridine-ortho was the highest among the six investigated systems, which was over ten times higher than that with carboxyl-para (the highest form among carboxyl anchors). NEGF-DFT calculations were used to elucidate the electron transport in the pyridine-based device and the carboxyl-based device. It was found that the electric current in the pyridine-based device was higher compared to that in the carboxyl-based device. In the case of the pyridine-based device, the transmission spectra at the applied bias showed that two peaks entered the bias window due to the strong electron transfer in the conducting channel, contributing to the high oscillator strength and enhanced catalytic activity.



The results imply the promising design of utilizing a pyridine anchor for the EY / anatase cluster compared to the carboxyl anchor. Experimental validations support this design strategy in good agreement. In particular, by modifying TiO₂ with para pyridine MY, AQY for H₂ and NH₃ formation under irradiation of 520 nm visible light was achieved ca. 2 and 0.67 % under addition of sacrificial agent, respectively. No decrease in activity over three times repetition suggesting pyridine linker is effective not only for charge transfer but also stable adsorption on anatase. This study demonstrated that molecular design for modified dye by DFT and NEGT-DFT calculation is highly efficient and effective for finding new organic dye with more efficient charge transfer.

ASSOCIATED CONTENT

The following files are available free of charge. Atomic coordinates of the optimized ortho, meta, para isomers of EY anchored by the carboxyl group as well as pyridine group on anatase, and the total energies of the isolated EY / anatase.

NOTES

The authors declare no competing financial interest.

ACKNOWLEDGMENT

This study was financially supported by Mitsui Chemical Inc Carbon Neutral Research Center (MCI-CNRC). All authors acknowledge the support of the World Premier International Research Center Initiative (WPI), Ministry of Education, Culture, Sports, Science, and Technology of Japan (MEXT).

REFERENCES



- (1) Yue, M.; Lambert, H.; Pahon, E.; Roche, R.; Jemei, S.; Hissel, D. Hydrogen Energy Systems: A Critical Review of Technologies, Applications, Trends and Challenges. *Renew. Sust. Energ. Rev.* **2021**, *146*, 111180.
- (2) Le, P.-A.; Trung, V. D.; Nguyen, P. L.; Phung, T. V. B.; Natsuki, J.; Natsuki, T. The Current Status of Hydrogen Energy: An Overview. *RSC Adv.* **2023**, *13*, 28262–28287.
- (3) Dawood, F.; Anda, M.; Shafiullah, G. M. Hydrogen Production for Energy: An Overview. *Int. J. Hydrogen Energy* **2020**, *45*, 3847–3869.
- (4) El-Emam, R. S.; Özcan, H. Comprehensive Review on the Techno-Economics of Sustainable Large-Scale Clean Hydrogen Production. *J. Clean. Prod.* **2019**, *220*, 593–609.
- (5) Fujishima, A.; Honda, K. Electrochemical Photolysis of Water at a Semiconductor Electrode. *Nature* **1972**, *238*, 37–38.
- (6) Tong, H.; Enomoto, N.; Inada, M.; Tanaka, Y.; Hojo, J. *Mater. Lett.* **2015**, *141*, 259–262.
- (7) Nishioka, S.; Yanagisawa, K.; Lu, D. T.; Vequizo, J. J. M.; Yamakata, A.; Kimoto, K.; Inada, M.; Maeda, K. *Sustain. Energ. Fuels* **2019**, *3*, 2337–2346.
- (8) Abe, R.; Hara, K.; Sayama, K.; Domen, K.; Arakawa, H. Steady Hydrogen Evolution from Water on Eosin Y-Fixed TiO₂ Photocatalyst Using a Silane-Coupling Reagent under Visible Light Irradiation. *J. Photochem. Photobiol. A* **2000**, *137*, 63–69.
- (9) Eidsvåg, H.; Bentouba, S.; Vajeeston, P.; Yohi, S.; Velauthapillai, D. TiO₂ as a Photocatalyst for Water Splitting—An Experimental and Theoretical Review. *Molecules* **2021**, *26*, 1687.
- (10) Liao, C.-H.; Huang, C.-W.; Wu, J. C. S. Hydrogen Production from Semiconductor-Based Photocatalysis via Water Splitting. *Catalysts* **2012**, *2*, 490–516.
- (11) Bledowski, M.; Wang, L.; Ramakrishnan, A.; Khavryuchenko, O. V.; Khavryuchenko, V. D.; Ricci, P. C.; Strunk, J.; Cremer, T.; Kolbeck, C.; Beranek, R. Visible-Light Photocurrent



Response of TiO₂–Polyheptazine Hybrids: Evidence for Interfacial Charge-Transfer Absorption. *Phys. Chem. Chem. Phys.* **2011**, *13*, 21511–21519.

(12) Murdoch, M.; Waterhouse, G. I. N.; Nadeem, M. A.; Metson, J. B.; Keane, M. A.; Howe, R. F.; Llorca, J.; Idriss, H. The Effect of Gold Loading and Particle Size on Photocatalytic Hydrogen Production from Ethanol over Au/TiO₂ Nanoparticles. *Nat. Chem.* **2011**, *3*, 489–492.

(13) Anpo, M.; Takeuchi, M. The Design and Development of Highly Reactive Titanium Oxide Photocatalysts Operating under Visible Light Irradiation. *J. Catal.* **2003**, *216*, 505–516.

(14) Li, Z.; Shi, L.; Franklin, D.; Koul, S.; Kushima, A.; Yang, Y. Drastic Enhancement of Photoelectrochemical Water Splitting Performance over Plasmonic Al@TiO₂ Heterostructured Nanocavity Arrays. *Nano Energy* **2018**, *51*, 400–407.

(15) Venturini, J.; Bonatto, F.; Guaglianoni, W. C.; Lemes, T.; Arcaro, S.; Alves, A. K.; Bergmann, C. P. Cobalt-Doped Titanium Oxide Nanotubes Grown via One-Step Anodization for Water Splitting Applications. *Appl. Surf. Sci.* **2019**, *464*, 351–359.

(16) Dong, Z.; Ding, D.; Li, T.; Ning, C. Ni-Doped TiO₂ Nanotubes Photoanode for Enhanced Photoelectrochemical Water Splitting. *Appl. Surf. Sci.* **2018**, *443*, 321–328.

(17) Sawant, S. Y.; Sayed, M. S.; Han, T. H.; Karim, M. R.; Shim, J.-J.; Cho, M. H. Bio-Synthesis of Finely Distributed Ag Nanoparticle-Decorated TiO₂ Nanorods for Sunlight-Induced Photoelectrochemical Water Splitting. *J. Ind. Eng. Chem.* **2019**, *69*, 48–56.

(18) Choi, W.; Termin, A.; Hoffmann, M. R. The Role of Metal Ion Dopants in Quantum-Sized TiO₂: Correlation between Photoreactivity and Charge Carrier Recombination Dynamics. *J. Phys. Chem.* **2002**, *98*, 13669–13679.

(19) Asahi, R.; Morikawa, T.; Ohwaki, T.; Aoki, K.; Taga, Y. Visible-Light Photocatalysis in Nitrogen-Doped Titanium Oxides. *Science* **2001**, *293*, 269–271.



- (20) Abe, R.; Takata, T.; Sugihara, H.; Domen, K. Photocatalytic Overall Water Splitting under Visible Light by TaON and WO₃ with an IO₃³⁻/I⁻ Shuttle Redox Mediator. *Chem. Comm.* **2005**, 30, 3829–3831.
- (21) Gao, Q.; Si, F.; Zhang, S.; Fang, Y.; Chen, X.; Yang, S. Hydrogenated F-Doped TiO₂ for Photocatalytic Hydrogen Evolution and Pollutant Degradation. *Inter. J. Hydrog. Energy* **2019**, 44, 8011–8019.
- (22) Elbakkay, M. H.; El Rouby, W. M.; El-Dek, S. I.; Farghali, A. A. S-TiO₂/S-Reduced Graphene Oxide for Enhanced Photoelectrochemical Water Splitting. *Appl. Surf. Sci.* **2018**, 439, 1088–1102.
- (23) Honda, Y.; Watanabe, M.; Hagiwara, H.; Ida, S.; Ishihara, T. Inorganic/Whole-Cell Biohybrid Photocatalyst for Highly Efficient Hydrogen Production from Water. *Appl. Catal. B Environ.* **2017**, 210, 400–406.
- (24) De Angelis, F. Direct vs. Indirect Injection Mechanisms in Perylene Dye-Sensitized Solar Cells: A DFT/TDDFT Investigation. *Chem. Phys. Lett.* **2010**, 493, 323–327.
- (25) Chu, W.; Chan, K. H.; Jafvert, C. T.; Chan, Y. S. Removal of Phenylurea Herbicide Monuron via Riboflavin-Mediated Photosensitization. *Chemosphere* **2007**, 69, 177–183.
- (26) Chen, C.; Qi, X.; Zhou, B. Photosensitization of Colloidal TiO₂ with a Cyanine Dye. *J. Photochem. Photobiol. A* **1997**, 109, 155–158.
- (27) Ibrahim, M. M.; Gaya, U. I.; Ibrahim, M. M.; Gaya, U. I. Synthesis of Eosin Y-sensitized Ag-TiO₂ Nano-hybrid for Optimized Photocatalytic Deradation of Aqueous Caffeine. *J. Chil. Chem. Soc.* **2019**, 64, 4275–4284.



(28) Wang, P.; Guan, Z.; Li, Q.; Yang, J. Efficient Visible-Light-Driven Photocatalytic Hydrogen Production from Water by Using Eosin Y-Sensitized Novel g-C₃N₄/Pt/GO Composites. *J. Mater. Sci.* **2018**, *53*, 774–786.

(29) Zhang, F.; Shi, F.; Ma, W.; Gao, F.; Jiao, Y.; Li, H.; Wang, J.; Shan, X.; Lu, X.; Meng, S. Controlling Adsorption Structure of Eosin Y Dye on Nanocrystalline TiO₂ Films for Improved Photovoltaic Performances. *J. Phys. Chem. C* **2013**, *117*, 14659–14666.

(30) Murakoshi, K.; Kano, G.; Wada, Y.; Yanagida, S.; Miyazaki, H.; Matsumoto, M.; Murasawa, S. Importance of Binding States between Photosensitizing Molecules and the TiO₂ Surface for Efficiency in a Dye-Sensitized Solar Cell. *J. Electroanal.* **1995**, *396*, 27–34.

(31) Nilsing, M.; Lunell, S.; Persson, P.; Ojamäe, L. Phosphonic Acid Adsorption at the TiO₂ Anatase (101) Surface Investigated by Periodic Hybrid HF-DFT Computations. *Surf. Sci.* **2005**, *582*, 49–60.

(29) Gillaizeau-Gauthier, I.; Odobel, F.; Alebbi, M.; Argazzi, R.; Costa, E.; Bignozzi, C. A.; Qu, P.; Meyer, G. J. Phosphonate-Based Bipyridine Dyes for Stable Photovoltaic Devices. *Inorg. Chem.* **2001**, *40*, 6073–6079.

(30) Zakeeruddin, S. M.; Nazeeruddin, M. K.; Pechy, P.; Rotzinger, F. P.; Humphry-Baker, R.; Kalyanasundaram, K.; Grätzel, M.; Shklover, V.; Haibach, T. Molecular Engineering of Photosensitizers for Nanocrystalline Solar Cells: Synthesis and Characterization of Ru Dyes Based on Phosphonated Terpyridines. *Inorg. Chem.* **1997**, *36*, 5937–5946.

(31) Ooyama, Y.; Nagano, T.; Inoue, S.; Imae, I.; Komaguchi, K.; Ohshita, J.; Harima, Y. Dye-sensitized Solar Cells Based on Donor- π -acceptor Fluorescent Dyes with a Pyridine Ring as an Electron-withdrawing-injecting Anchoring Group. *Chem. Eur. J.* **2011**, *17*, 14837–14843.



- (32) Perdew, J. P.; Burke, K.; Ernzerhof, M. Generalized, Gradient Approximation Made Simple. *Phys. Rev. Lett.* **1996**, 77, 3865–3868.
- (33) Becke, A. D. Density-functional Thermochemistry. I. The Effect of the Exchange-only Gradient Correction. *J. chem. phys.* **1992**, 96, 2155–2160.
- (34) Lee, C.; Yang, W.; Parr, R. G. Development of the Colle-Salvetti Correlation-Energy Formula into a Functional of the Electron Density. *Phys. Rev. B* **1988**, 37, 785.
- (35) Weigend, F.; Ahlrichs, R. Balanced Basis Sets of Split Valence, Triple Zeta Valence and Quadruple Zeta Valence Quality for H to Rn: Design and Assessment of Accuracy. *Phys. Chem. Chem. Phys.* **2005**, 7, 3297–3305.
- (36) Hay, P. J.; Wadt, W. R. Ab Initio Effective Core Potentials for Molecular Calculations. Potentials for the Transition Metal Atoms Sc to Hg. *J. Chem. Phys.* **1985**, 82, 270–283.
- (37) Cromer, D. T.; Herrington, K. The Structures of Anatase and Rutile. *J. Am. Chem. Soc.* **1955**, 77, 4708–4709.
- (38) Addamo, M.; Bellardita, M.; Di Paola, A.; Palmisano, L. Preparation and Photoactivity of Nanostructured Anatase, Rutile and Brookite TiO₂ Thin Films. *Chem. Commun.* **2006**, 47, 4943–4945.
- (39) Tay, Q.; Liu, X.; Tang, Y.; Jiang, Z.; Sum, T. C.; Chen, Z. Enhanced Photocatalytic Hydrogen Production with Synergistic Two-Phase Anatase/Brookite TiO₂ Nanostructures. *J. Phys. Chem. C* **2013**, 117, 14973–14982.
- (40) Tian, F. H.; Wang, X.; Zhao, W.; Zhao, L.; Chu, T.; Yu, S. Adsorption of 2-Propanol on Anatase TiO₂ (101) and (001) Surfaces: A Density Functional Theory Study. *Surf. Sci.* **2013**, 616, 76–84.



- (41) *TURBOMOLE V6.4*; TURBOMOLE GmbH: Karlsruhe, Germany, 2007; <http://www.turbomole.com>, 2007.
- (42) Datta, S. *Quantum Transport: Atom to Transistor*; Cambridge University Press: Cambridge, U.K., 2005.
- (43) *QuantumATK S-2021.06-SP2*; Quantumwise: Copenhagen, Denmark, 2021; <http://www.quantumwise.com>.
- (44) Kohn, W.; Sham, L. J. Self-Consistent Equations Including Exchange and Correlation Effects. *Phys. Rev.* **1965**, *140*, A1133–A1138.
- (45) Fuchs, M.; Scheffler, M. Ab Initio Pseudopotentials for Electronic Structure Calculations of Poly-Atomic Systems Using Density-Functional Theory. *Comput. Phys. Commun.* **1999**, *119*, 67–98.
- (46) Davidson, E. R.; Feller, D. Basis Set Selection for Molecular Calculations. *Chem. Rev.* **1986**, *86*, 681–696.
- (47) Liu, X.; Huang, W.; Lei, Y.; Li, Y.; Xue, Y.; Wang, F.; Min, S. Effective Hydrothermal Grafting of Eosin Y onto TiO₂ Nanoparticles Towards Stable Photocatalysts for Efficient Visible-Light-Driven Photocatalytic H₂ Evolution. *New J. Chem.* **2018**, *42*, 6631–6635.
- (48) Kosem, N.; Watanabe, M.; Song, J. T.; Takagaki, A.; Ishihara, T. A Comprehensive Study on Rational Biocatalysts and Individual Components of Photobiocatalytic H₂ Production Systems. *Appl. Catal. A Gen.* **2023**, *651*, 119019.
- (49) Kosem, N.; Shen, X.-F.; Ohsaki, Y.; Watanabe, M.; Song, J. T.; Ishihara, T. Photobiocatalytic Conversion of Solar Energy to NH₃ from N₂ and H₂O under Ambient Condition. *Appl. Catal. B Environ.* **2024**, *342*, 123431.



(50) Kosem, N.; Honda, Y.; Watanabe, M.; Takagaki, A.; Tehrani, Z. P.; Haydous, F.; Lippert, T.; Ishihara, T. Photobiocatalytic H₂ Evolution of GaN:ZnO and [FeFe]-Hydrogenase Recombinant *Escherichia coli*. *Catal. Sci. Technol.* **2020**, *10*, 4042–4052.

(51) Hirakawa, H.; Hashimoto, M.; Shiraishi, Y.; Hirai, T. Photocatalytic Conversion of Nitrogen to Ammonia with Water on Surface Oxygen Vacancies of Titanium Dioxide, *J. Am. Chem. Soc.* **2017**, *139*, 10929–10936.

(52) Zhang, L.; Liu, X.; Rao, W.; Li, J. Multilayer Dye Aggregation at Dye/TiO₂ Interface via π - π Stacking and Hydrogen Bond and Its Impact on Solar Cell Performance: A DFT Analysis. *Sci Rep.* **2016**, *6*, 35893.

(53) Zhang, L.; Cole, J. M. Adsorption Properties of P-Methyl Red Monomeric-to-Pentameric Dye Aggregates on Anatase (101) Titania Surfaces: First-Principles Calculations of Dye/TiO₂ Photoanode Interfaces for Dye-Sensitized Solar Cells. *ACS Appl. Mater. Interfaces* **2014**, *6*, 15760–15766.

(54) Labat, F.; Ciofini, I.; Hratchian, H. P.; Frisch, M.; Raghavachari, K.; Adamo, C. First Principles Modeling of Eosin-Loaded ZnO Films: A Step toward the Understanding of Dye-Sensitized Solar Cell Performances. *J. Am. Chem. Soc.* **2009**, *131*, 14290–14298.

(55) De Angelis, F.; Di Valentin, C.; Fantacci, S.; Vittadini, A.; Selloni, A. Theoretical Studies on Anatase and Less Common TiO₂ Phases: Bulk, Surfaces, and Nanomaterials. *Chem. Rev.* **2014**, *114*, 9708–9753.

(56) Ie, Y.; Hirose, T.; Nakamura, H.; Kiguchi, M.; Takagi, N.; Kawai, M.; Aso, Y. Nature of Electron Transport by Pyridine-Based Tripodal Anchors: Potential for Robust and Conductive Single-Molecule Junctions with Gold Electrodes. *J. Am. Chem. Soc.* **2011**, *133*, 3014–3022.



(57) Li, X.; Cao, L.; Li, H.-L.; Wan, H.; Zhou, G. Spin-Resolved Transport Properties of a Pyridine-Linked Single Molecule Embedded between Zigzag-Edged Graphene Nanoribbon Electrodes. *J. Phys. Chem. C* **2016**, *120*, 3010–3018.

(58) Kamenetska, M.; Quek, S. Y.; Whalley, A. C.; Steigerwald, M. L.; Choi, H. J.; Louie, S. G.; Nuckolls, C.; Hybertsen, M. S.; Neaton, J. B.; Venkataraman, L. Conductance and Geometry of Pyridine-Linked Single-Molecule Junctions. *J. Am. Chem. Soc.* **2010**, *132*, 6817–6821.

(59) Adak, O.; Korytár, R.; Joe, A. Y.; Evers, F.; Venkataraman, L. Impact of Electrode Density of States on Transport through Pyridine-Linked Single Molecule Junctions. *Nano Lett.* **2015**, *15*, 3716–3722.

(60) Son, H.-O.; Prasittichai, C.; Mondloch, J. E.; Luo, L.; Wu, J.; Kim, D. W.; Farha, O. K.; Hupp, J. T., Dye Stabilization and Enhanced Photoelectrode Wettability in Water-Based Dye-Sensitized Solar Cells through Post-assembly Atomic Layer Deposition of TiO₂. *J. Am. Chem. Soc.* **2013**, *135*, 11529–11532.

(61) Willkomm, J.; Orchard, K. L.; Reynal, A.; Pastor, E.; Durrant, J. R.; Reisner, E. Dye-Sensitised Semiconductors Modified with Molecular Catalysts for Light-Driven H₂ Production. *Chem. Soc. Rev.* **2016**, *45*, 9–23.

(62) van der Ham, C. J. M.; Koper, M. T. M.; Hetterscheid, D. G. H. Challenges in Reduction of Dinitrogen by Proton and Electron Transfer. *Chem. Soc. Rev.* **2014**, *43*, 5183–5191.

(63) Muro-Pastor, M. I.; Florencio, F. J. Regulation of Ammonium Assimilation in Cyanobacteria. *Plant Physiol. Biochem.* **2003**, *41*, 595–603.

(64) Wang, L.; Xia, M.; Wang, H.; Huang, K.; Qian, C.; Maravelias, C. T.; Ozin, G. A. Greening Ammonia Toward the Solar Ammonia Refinery. *Joule* **2018**, *2*, 1055–1074.



(65) Boucher, D. G.; Carroll, E.; Nguyen, Z. A.; Jadhav, R. G.; Simoska, O.; Beaver, K.; Minteer, S. D. Bioelectrocatalytic Synthesis: Concepts and Applications. *Angew. Chem. Int. Ed.* **2023**, *62*, e202307780.

(66) Sengupta, K.; Joyce, J. P.; Decamps, L.; Kang, L.; Bjornsson, R.; Rüdiger, O.; DeBeer, S. Investigating the Molybdenum Nitrogenase Mechanistic Cycle Using Spectroelectrochemistry. *J. Am. Chem. Soc.* **2025**, *147*, 2099–2114.



Data statement

Improved Charge Transfer Performance of Eosin Y-Sensitized Anatase TiO₂ by Anchoring Group Modification: from the Theory to Experiment

Juan Shang,^{1,2,3,} Nuttavut Kosem,^{1,2} Yasuhiro Kayo,⁴ Xiao-Feng Shen,¹ Sayo*

Matsuyama,¹ Motonori Watanabe,^{1,2,4} Miki Inada,¹ Tatsumi Ishihara,^{1,2,4}

*and Aleksandar Staykov^{1,2,**}*

All data is available upon request from the corresponding author.

